13. B. Millard et al, *J. Phys. Chem.*, **59**, 976(1955).
14. W. D. Harkins, Physical Chemistry of surface Films (Reinhold Publishing Corp., 1957).
15. S. Brunauer, Physical Adsorption (Princeton Univ. Press, 1945).
16. I. Langmuir, *J. Am. Chem. Soc.*, **40**, 1361 (1918).
17. W. A. Steele and G. D. Jr. Halsey, *J. Chem Phys.*, 22, 979 (1954); *J. Phys. Chem.*, **59**, 57 (1955); N. P. Freeman and G. D. Jr. Halsey, *ibid*, **59**, 181 (1955); G. Constabaris and G. D., Jr., Halsey, *J. Chem. Phys.*, **27**, 1434 (1957).
18. S. Ross and J. P. Olivier, *J. Phys. Chem.*, **63**, 608 (1961); On Physical Adsorption (Interscience Publishing Comp., New York, 1964).
19. W. A. Steele, Solid Surfaces and the Gas Solid Interface (Adv. in Chem. Ser. 33, *Am. Chem. Soc.*, Washington, D. C., 1961).
20. D. M. Young and A. D. Crowell, Physical Adsorption of Gases (Butterworth, Washington, D. C., Ist ed., 1962).
21. S. Chang and H. Pak, *J. Korean Chem. Soc.*, **14**, 111 (1970).
22. Herzberg, Infrared and Raman Spectra (D. Van Nostrand Comp. Ltd., 0th printing, 1962).
23. M. Hughes, Physical Chemistry (Pergamon Press, Inc., New York, 1961).
24. F. T. Miles and A. W. C. Mengie, *J. Am. Chem. Soc.*, **58**, 1069 (1936).
25. Tsing-Lien Chang and Jen-Yuan Chien, *J. Am. Chem. Soc.*, **63**, 1709 (1941); Tsing-Lien Chang and Lu-Ho Tung, Nature, **163**, 737 (1949).
26. (a) B. L. Baker, U. S. Energy Comm., AECU 4738, 50pp (1959); (b) I. Kirshenbaum, Physical Properties and Analysis of Heavy Water Nat. Nuc. Energy Ser. (McGraw-Hill Book Comp., Inc., New York 1951).
27. G. D. Oliver and J. W. Grisard, *J. Am. Chem. Soc.*, **78**, 561 (1951).
28. J. W. McBain, *J. Am. Chem. Soc.*, **55**, 2294 (1933).
29. C. C. Horton and L. E. J. Roberts, Atomic Energy Research Estab. (Gt Brit), C/R 2219, 23 (1958). ; *Chem. Abs.*, 15186e (1958).
30. A. C. Zettlemoyer et al, *J. Phys. Chem.*, **5**, 313 (1954)

DAEHAN HWAHAK HWOEJEE
(Journal of the Korean Chemical Society)
Vol. 15, No. 6, 1971
Printed in Republic of Korea

# Kinetics of Thixotropy of Aqueous Bentonite Suspension

**Kisoon Park*** and **Taikyue Ree**

*Department of Chemistry, University of Utah, Salt Lake City, Utah, U. S. A.*

(Received Oct. 21, 1971)

**Abstract** The rheological properties of aqueous suspensions of Black Hills bentonite were measured by using a Couette-type viscometer. Three kinds of flow units in aqueous bentonite suspension were postulated. Each has a different average relaxation time, one Newtonian and the other two non-Newtonian. One of the non-Newtonian types is thixotropic, and the other is non-thixotropic. The thixotropic non-Newtonian unit is transformed to a Newtonian unit by shear stress. If the stress is relieved, the transformed unit returns to its original state. Two flow equations were derived by introducing chemical kinetics consideration for such a transition into the generalized theory of viscous flow. One equation describes the "upcurve," a diagram of rate of shear versus shear stress, obtained by increasing the rate of shear, and the other relates to the "downcurve"

* Present Address: Union Carbide Corporation, Chemicals and Plastics Division, South Charleston, W. Va., U. S. A.

obtained by decreasing the shear rate. The equations satisfactorily describe the experimental thixotropic hysteresis of bentonite suspensions. The equations also were successfully applied to the flow curves of the suspensions containing various amounts of monovalent electrolyte (KCl).

## Introduction

It is well known that thixotropy preferentially occurs in sols or suspension containing plate-shaped or rod-shaped particles such as ferric oxide, vanadium pentoxide and many clay minerals. The montmorillonites to which the bentonite clay belongs have a layer structure composed of extremely small platelets,[1-3] and their aqueous suspension exhibits pronounced thixotropic properties. Thus the thixotropy of bentonite suspension has been a frequent subject of experimental investigations.[4-10] These studies, however, are mostly phenomenological, the relationship between structure in suspension and flow behavior is not clearly understood. In the present study, an attempt has been made to illucidate thixotropy from the view point of chemical kinetics. Thixotropy here is defined as the phenomenon having the following characteristics: (1) It accompanies an isothermal structural change which is brought about by disturbing a system mechanically; (2) When the disturbance is ceased, the system recovers its original structure; (3) The flow curve (shear rate versus shear stress) of the system has a hysteresis loop. The experimentally determined hysteresis loops were described by an equation which is a modified form of the theory of thixotropy advanced by Hahn, Ree and Eyring,[11a] and Utsugi, Iwasawa and Ree.[11b]

## Experimental

The bentonite studied was Black Hills montmorillonite furnished by the International Minerals and Chemical Corporation through the Brumley Donaldson Company, Los Angeles, California. The chemical composition was: silica, 64.72%; alumina, 20.82%; iron oxide, 3.44%; titanium oxide, 0.14%; lime, 0.49%; magnesia, 2.38%; and alkalis, 2.92%.

Various methods of mixing the bentonite with distilled water were tested. In order to prepare suspensions yielding reproducible flow data, a Cenco stirrer with a paddle of constant shape was used throughout the experiment. Three hours of mixing at 635 rpm gave a satisfactorily uniform suspension.

The suspensions containing various amounts of salt were prepared by the following procedure: a desired amount of bentonite suspension was mixed with a measured amount of 0.1 $N$ potassium chloride solution, and the final electrolyte concentration was adjusted by adding distilled water.

The apparatus used in measuring the flow curves was a Couette-type rotational viscometer which is similar to the Green-Weltman viscometer.[12,13a] The main features of the viscometer were reported elsewhere.[13b] The number of revolutions of the cup per second was controlled by a variable speed transmission which gave a uniform variation of shear rate from zero up to 4500 $sec^{-1}$ by a proper selection of gear and cylinder sets. All the measurements were done with a cylinder set having a ratio ($R_b/R_c$) of 0.855, where $R_b$ and $R_c$ are radii of the bobbin and the cup. A constant-temperature water bath with a precision micro-set differential thermoregulator controlled temperature on the cup surface to within about 0.2°C.

## Experimental Results

*Figure* 1 represents a typical flow curve (shear

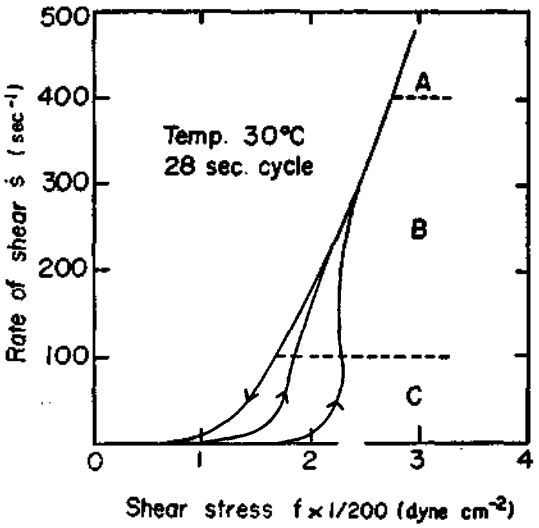


*Fig.* 1. Flow curves of 10 wt. % aqueous bentonite suspension.

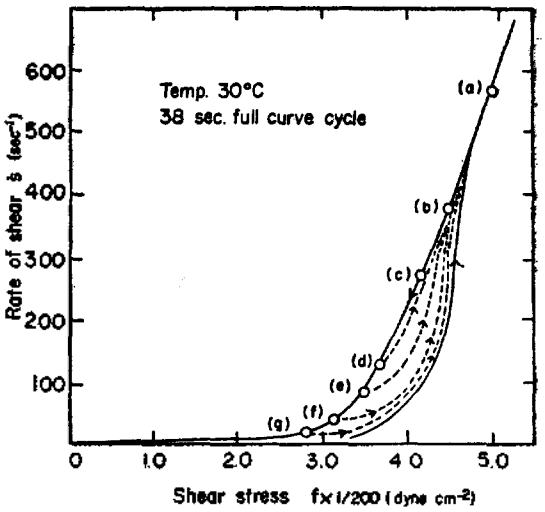


*Fig.* 2. Scanning curves for the suspension of 10.5 wt. % bentonite.

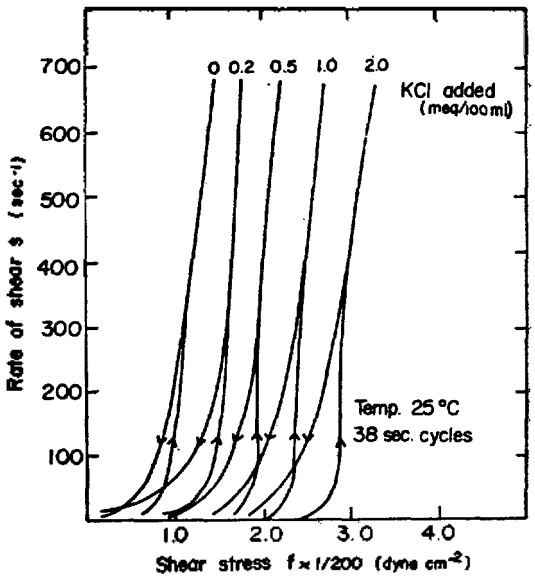


*Fig.* 3. Hysteresis loops of 9.0 wt. % bentonite suspension containing various amounts of KCl.

rate $\dot{s}$ versus shear stress $f$) of aqueous suspension of bentonite. The sample contained in the viscometer cup was rested for 6 hours prior to the measurement. The upward arrow indicates the "upcurve" obtained by increasing the rate of shear from zero to the maximum shear rate and the downward arrow indicates the "downcurve" obtained while the rate of shear was decreased from the maximum to zero. The smaller hysteresis loop appearing inside the larger one is a reproducible curve which was obtained by a repeated cyclic deformation. The size of the hysteresis loop obtained from the initial cyclic deformation was markedly dependent on the rest period of the sample, *i.e.*, the longer the rest period, the larger was the hysteresis loop. The size of the reproducible loop, however, was independent of the resting time.

The full curve in *Fig.* 2 is a reproducible hysteresis loop of 10.5 wt. % suspension. The following experiment was conducted with the sample: At a point labelled "*a*" on the downcurve, the shear rate was increased and the upcurve was obtained. The upcurve thus obtained retracted the downcurve. After the upcurve reached the apex, the shear rate was immediately decreased to make the downcurve. This procedure produced the downcurve coinciding with the original downcurve, *i.e.*, the

scanning up and down curve yielded no hysteresis loop. Similar experiments were performed at points "*b*" and "*c*", but no appreciable hysteresis was observed. Further scanning experiments made in order at points *d*, *e*, and *f*, however, produced hysteresis loops. Furthermore, the lower the point at which the scanning upcurve was made the larger was the loop. It is seen that the loop originated from the scanning point *f*, is significantly larger than that originated from point *d* (see *Fig.* 2). The scanning up and down curve from the point *g* almost reproduced the original loop (full curve). The scanning downcurve was independent of the scanning points from which the scanning upcurves were obtained. Each scanning curve was brought clear down to the zero shear rate, after which the upcruve was immediately determined each time before reaching the "scanning points" *a* to *g*.

*Fig.* 3 represents the variation with electrolyte concentration of the reproducible hysteresis loop for 9.0 wt. per cent bentonite suspension containing potassium chloride. The concentration of KCl ranged from zero to 2.0 meq./100 ml. It is shown that the increase in electrolyte concentration shifts the flow curve to the higher stress region. Furthermore, the hysteresis loop became larger as the electrolyte concentration increased.

## Analyses and Discussion

**The Generalized Equation of Viscous Flow** A non-Newtonian system is composed of flow units of different relaxation times in the generalized theory of viscous flow.[14] The viscosity $\eta$, defined as $f/\dot{s}$ ($f$ is the shear stress and $\dot{s}$ the rate of shear) is expressed by the following equation,

$$\eta=\sum_{n=1}^{n}\frac{X_n\beta_n}{\alpha_n}\ \frac{\sinh^{-1}\beta_n\dot{s}}{\beta_n\dot{s}} \qquad (1)$$

where $\beta_n$ is a quantity proportional to the relaxation time of the $n$th type flow unit, $X_n$ is the fraction of area occupied by the $n$th type flow units on a shear surface and $\alpha_n$ is a parameter, the reciprocal of which is proportional to the shear modulus of type $n$ unit. The parameters $\beta_n$ and $\alpha_n$ have the following relations:

$$\beta_n=\left(\frac{\lambda}{\lambda_1}2k'\right)_n^{-1} \qquad (2)$$

and

$$\alpha_n=\left(\frac{\lambda\lambda_2\lambda_3}{2kT}\right)_n \qquad (3)$$

where $\lambda$, $\lambda_1$, $\lambda_2$ and $\lambda_3$ are the molecular dimensions,[14] and $k'$ is the specific rate constant, $k$ the Boltzman constant, and $T$ the absolute temperature. For briefness, $\beta_n$ and $1/\alpha_n$ are called here the intrinsic relaxation time and the intrinsic shear modulus of type $n$ unit ($n$=1, 2, 3···), respectively.

**Flow Equation for Bentonite Suspension** It is reasonable to suggest four different particle arrangements in a suspension of platelike clay particles. The arrangements are edge-to-edge, face-to-face, edge-to-face associations and one in which the particles are arranged in more or less parallel fashion without having any contact between the particles. Sodium bentonite swells in the presence of water, and the plate-like particles separate into individual layers or into stacks of several layers.[3,15,16] This swelling and subsequent separation of platelets could form an extensive "card-house" structure through the arrangements of platelike particles mentioned above.

Bentonite particles have two crystallographically different surfaces that carry different charges; the surfaces are negatively charged and the edges carry positive charges.[17] Thus, the edge-to-face interaction is a preferred form of interaction leading to the scaffolding of the

card-house structure. Edge-to-edge interaction yields a much weaker structure than the edge-to-face interaction since the former involves the similar surface charges on the edges.

Bates[3] observed that the sheets approaching a thickness of one or two unit layers (10 to 30Å) are to be common for Wyoming bentonite dispersed in water. The face area of bentonite flakes are estimated to be in the order of 10 to 100 times the thickness of the flakes.[2]

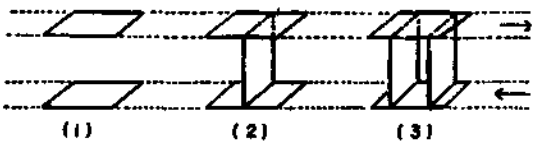


*Fig.* 4. Flow units for bentonite suspension.

The following analysis assumes three types of flow units, illustrated in *Fig.* 4, in bentonite suspension. In the first type, flakes of bentonite flow past each other, lubricated by the suspending fluid. In type 2 and 3, the two parallel flakes are bonded together by one and two flakes, respectively, through the face-to-edge interaction. The units of type 1 flow easily. The type 2 units, under the influence of shear stress, transform readily to type 1 units. The flow units of type 3 are not readily destroyed, but when they do, recover the original structure rapidly so that their concentration is unaffected by the rate of flow. In addition to the three types, many other types of units differing in shape as well as in the values of $\alpha$ and $\beta$ from those represented in *Fig.* 4 are possible. These units, however, may be regarded as variations of the three types discussed. For example, a flow unit where the bentonite flakes are linked by edge-to-edge interactions may be classified to the type 2 unit. As mentioned previously, all these types of flow units contribute to the scaffolding structure of bentonite suspension.

Let $f_1$, $f_2$ and $f_3$ be the stresses acting on type 1, 2, and 3 units, respectively. The quantities, $X_n$, $\beta_n$ and $1/\alpha_n$ ($n$=1. 2, 3) have already been defined. As previously mentioned, even in a given type of flow units, there are several variations; thus, the values of $\alpha_n$, $\beta_n$ and $X_n$ ($n$=1, 2, 3) may be considered as the averages for each type of flow units. This kind of consideration is justified by the fact that bentonite suspensions are a polydispersed system.[18,19]

The following relations hold:

$$X_1+X_2+X_3=1 \tag{4}$$

and

$$f=X_1f_1+X_2f_2+X_3f_3 \tag{5}$$

where $f$ is the total shear stress. By introducing Eqs. (4) and (5) into (1), one obtains the flow equation for the bentonite suspension as follows:

$$\eta=\frac{X_1\beta_1}{\alpha_1}+\frac{X_2\beta_2}{\alpha_2}\frac{\sinh^{-1}\beta_2\dot{s}}{\beta_2\dot{s}}+\frac{X_3\beta_3}{\alpha_3}\frac{\sinh^{-1}\beta_3\dot{s}}{\beta_3\dot{s}} \tag{6}$$

$$f=\frac{X_1\beta_1}{\alpha_1}\dot{s}+\frac{X_2}{\alpha_2}\sinh^{-1}\beta_2\dot{s}+\frac{X_3}{\alpha_3}\sinh^{-1}\beta_3\dot{s} \tag{7}$$

where type 1 is assumed to be Newtonian.[14]

**Transition Between Type 2 and 1 Units**

According to the theory of rate processes,[14,20] the rate of transition from type 2 to type 1 units is given by;

$$-\frac{dX_2}{dt}=X_2k_f\exp(w/2kT)-X_1k_b\exp(-w/2kT) \tag{8}$$

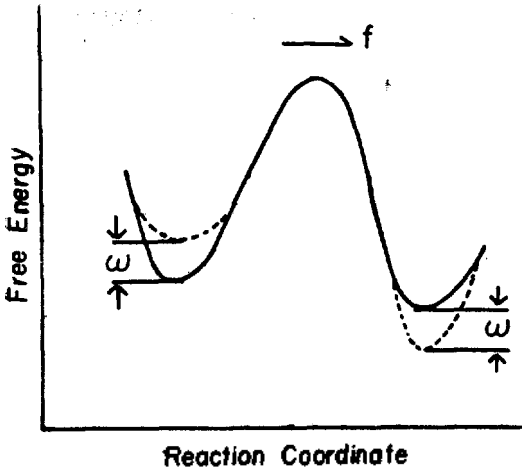


*Fig.* 5. Free energy diagram for the transition of type 2 flow unit to type 1 unit.

The rate constants $k_f$ and $k_b$ are for the forward and backward reactions, of type 2 ⇆ type 1, when no stress acts on the system; $w$ is the work done by the stress on type 2 unit, the activation free energy for forward reaction $\Delta F_f^*$ decreases by $w$ while $\Delta F_b^*$ for the reverse reaction increases by the same amount of work (*Fig.* 5). The work $w$ stored as elastic energy can be expressed as

$$w=\int_0^s Gsds=Gs^2/2 \tag{9}$$

where $s$ is the shear, and $G$ is the elasticity constant. Since shear continues until one flake of type 2 unit breaks away from its counterpart in the neighboring layer, the upper limit of the integration will be $s=\dot{s}/k_f$.[11] Thus,

$$w=G\dot{s}^2/2k_f^2=2c\dot{s}^2 \tag{10}$$

where

$$c=G/4k_f^2 \tag{11}$$

Substituting Eq. (10) into (8) yields

$$-\frac{dX_2}{dt}=X_2k_f\exp(c\dot{s}^2/kT) - X_1k_b\exp(-c\dot{s}^2/kT) \tag{12}$$

Since the total sum of $X_1$ and $X_2$ is constant, *i.e.*,

$$X_1+X_2=C' \tag{13}$$

Eq. (12) can be rewritten as;

$$-\frac{dX_2}{dt}=X_2[k_f\exp(c\dot{s}^2/kT)+k_b\exp(-c\dot{s}^2/kT)]-C'k_b\exp(-c\dot{s}^2/kT) \tag{14}$$

Using the experimental relation between $\dot{s}$ and time $t$,

$$\dot{s}=\rho t, \tag{15}$$

(where $\rho$ is a constant) the solution of Eq. 14 is found:

$$X_2=\exp[-(k_f\gamma I+k_b\gamma I')] [C'k_b\gamma\int_0^y\exp(-y^2)\exp(k_f\gamma I+k_b\gamma I')dy+X_2^{(\infty)}] \tag{16}$$

where

$$I=\int_0^y\exp(y^2)dy \tag{17a}$$

$$I'=\int_0^y\exp(-y^2)dy \tag{17b}$$

$$y=(c\dot{s}^2/kT)^{\frac{1}{2}}=\dot{s}/\gamma\rho=t/\gamma \tag{17c}$$

$$\gamma=(kT/c\rho^2)^{\frac{1}{2}} \tag{17d}$$

and $X_2^{(\infty)}$ is the quantity of $X_2$ at $\dot{s}=0$.

Equation(14) also applies to the downcurve. But in this case, the following relations should hold:

$$\dot{s}_m-\dot{s}=\rho t \tag{18a}$$

$$y_m-y=t/\gamma \tag{18b}$$

where $\dot{s}_m$ is the shear rate at the apex, $y_m$ is the corresponding quantity of $y$ at the apex of the cyclic curve, and $t$ is measured starting from the apex. The solution of Eq. (14) for the

downcurve is then given by

$$X_2=\exp[-(k_f\gamma J+k_b\gamma J')]$$
$$[C'k_b\gamma\int_{y'}^{y_\infty}\exp(-y'^2)\exp(k_f\gamma J+k_b\gamma J')dy'+X_2^{(m)}] \tag{19}$$

where

$$J=\int_{y'}^{y_\infty}\exp(y'^2)dy' \tag{20a}$$
$$J'=\int_{y'}^{y_\infty}\exp(-y'^2)dy' \tag{20b}$$
$$y'=\dot{s}_m/\gamma\rho-t/\gamma \tag{20c}$$

and $X_2^{(m)}$ is the $X_2$ at $\dot{s}=\dot{s}_m$. When relation (13) is introduced into Eq. (7) and rearranged, an expression for $f$ is obtained

$$f=\frac{C'\beta_1}{\alpha_1}\dot{s}+\frac{X_3}{\alpha_3}\sinh^{-1}\beta_3\dot{s}$$
$$+\frac{X_2}{C'}\left(\frac{C'\sinh^{-1}\beta_2\dot{s}}{\alpha_2}-\frac{C'\beta_1\dot{s}}{\alpha_1}\right) \tag{21}$$

By introducing Eq. (16) into (21) the upcurve expression is derived:

$$f=\frac{C'\beta_1}{\alpha}\dot{s}+\frac{X_3}{\alpha_3}\sinh^{-1}\beta_3\dot{s}+\left[\frac{C'}{\alpha_2}\sinh^{-1}\beta_2\dot{s}-\frac{C'\beta_1}{a_1}\dot{s}\right]\exp[-k_f\gamma I+k_b\gamma I')]$$
$$\left[k_b\gamma\int_0^{y'}\exp(-y^2)\exp(k_f\gamma I+k_b\gamma I')dy+\frac{X_2^{(0)}}{C'}\right] \tag{22}$$

Similarly, the equation for the downcurve is obtained by combing Eqs. (21) and (16), *i.e.*,

$$f=\frac{C'\beta_1}{\alpha_1}\dot{s}+\frac{X_3}{\alpha_3}\sinh^{-1}\beta_3\dot{s}+\left(\frac{C'}{\alpha_2}\sinh^{-1}\beta_2\dot{s}-\frac{C'\beta_1}{\alpha_1}\dot{s}\right)\exp[-(k_f\gamma J+k_b\gamma J')]$$
$$\left[k_b\gamma\int_{y'}^{y_\infty}\exp(-y'^2)\exp(k_f\gamma J+k_b\gamma J')dy'+\frac{X_2^{(0)}}{C'}\right] \tag{23}$$

**Determination of the Parameters** Scanning experiments have shown that appreciable recovery of the bentonite suspension does not occur until the shear rate decreases below 200 $sec^{-1}$ in downcurves (*Fig.* 2). In accord with this observation, the following equation is applied to the downcurves above $\dot{s}=200$ $sec.^{-1}$,

$$f=\frac{C'\beta_1}{\alpha_1}\dot{s}+\frac{X_3}{\alpha_3}\sinh^{-1}\beta_3\dot{s} \tag{24}$$

where it is assumed that all type 2 units are transformed to type 1 units. The values of $C'\beta_1/\alpha_1$, $X_3/\alpha_3$ and $\beta_3$ are thus obtained from downcurves above $\dot{s}=200$ $sec^{-1}$. Because of the above-mentioned observed fact, the recovery term (the reverse reaction) in Eq. (12) is neglected above $\dot{s}=200$ $sec^{-1}$, *i.e.*,

$$-\frac{dX_2}{dt}=X_2k_f\exp(c\dot{s}^2/kT) \tag{25}$$

The solution of this equation is:

$$X_2=X_2^{(0)}\exp(-k_f\gamma I) \tag{26}$$

Substituting Eq. (26) into Eq. (21) provides the following equation for the upcurve above $\dot{s}=200$ $cm^{-1}$:

$$f=\frac{C'\beta_1}{\alpha_1}\dot{s}+\frac{X_3}{\alpha_3}\sinh^{-1}\beta_3\dot{s}+\frac{X_2^{(0)}}{C'}\cdot$$
$$\exp(-k_f\gamma I)\left(\frac{C'}{\alpha_2}\sinh^{-1}\beta_2\dot{s}-\frac{C'\beta_1}{\alpha_1}\dot{s}\right) \tag{27}$$

The constant $X_2^{(0)}/C'$ was estimated from Eq. (14) by assuming that $X_2$ is about constant,

*i.e.*, $-dX_2/dt \simeq 0$ when $\dot{s}$ is very small. It may also be assumed that $k_f \simeq k_b$. The latter assumption is made since the recovery reaction is very rapid as $\dot{s}$ approaches zero. Thus, the following relation is obtained from Eq. (14):

$$X_2^{(0)} = C' \Big/ \left[\frac{k_f}{k_b}\exp(2c\dot{s}^2/kT)+1\right] \simeq C' \Big/ \left(\frac{k_f}{k_b}+1\right) \simeq C'/2 \quad (28)$$

or $$X_2^{(0)}/C' \simeq 0.5 \quad (29)$$

Of course, this value is not exact because of the assumptions involved in its evaluation, but it serves in obtaining a better value of $X_2^{(0)}/C'$ which will be mentioned shortly.

The values of $C'/\alpha_2$ and $\beta_2$ were obtained by applying Eq. (21) to the region of $\dot{s}$ (0 to 100 $sec^{-1}$) of upcurve assuming $X_2/C' \simeq X_2^{(0)}/C' \simeq 0.5$.

Rearranging Eq. (27) gives

$$\frac{f - \frac{C'\beta_1}{\alpha_1}\dot{s} - \frac{X_3}{\alpha_3}\sinh^{-1}\beta_3\dot{s}}{\frac{X_2^{(0)}}{C'}\left(\frac{C'}{\alpha_2}\sinh^{-1}\beta_2\dot{s} - \frac{C'\beta_1}{\alpha_1}\dot{s}\right)} = \exp(-k_f\gamma I) \quad (30)$$

The left-hand side of Eq. (30) is calculated at a point ($f$, $\dot{s}$) by using parametric values thus far obtained, hence $k_f\gamma I$ is calculable. Let the values of $k_f\gamma I$ at point 1 ($f_1$, $\dot{s}_1$) and point 2 ($f_2$, $\dot{s}_2$) be $(k_f\gamma I)_1$ and $(k_f\gamma I)_2$, respectively. Then one obtains the following relation:

$$\frac{(k_f\gamma I)_1}{(k_f\gamma I)_2} = \frac{I_1}{I_2} \quad (31)$$

which is a function of $(\dot{s}_1/\dot{s}_2)$.

On the one hand, the numerical values of $I$ for different values of of $y(=\dot{s}/\gamma\rho)$ were calculated, and tabulated by using a computer. From the *Table*, the two values of $I_1$ and $I_2$ are found whose ratio satisfies Eq. (31). Consequently, the values of $y_1$ and $y_2$ corresponding to the two given values of $\dot{s}_1$ and $\dot{s}_2$ are found from the table. Since $y_1 = \dot{s}_1/\gamma\rho$ and $\rho = 36$ in our experiment, $\gamma$ can be calculated.

The value of $k_f$ can also be determined from the known values of $(k_f\gamma I)_1$, and $(k_f\gamma I)_2$, since the values of $I_1$, $I_2$ and $\gamma$ are known. The value of $k_b$ was obtained by adjusting the values of $k_b$ in Eq. (22) so that the best fit of the upcurve was obtained. When the value of $k_f$ thus determined was introduced into Eq. (27) to deduce the value of $X_2^{(0)}/C'$, it was found to be 0.45, which was a little smaller than the previously estimated value 0.5 [Eq. (29)].

By repeating the above procedure, the best values of all the parameters entering into Eqs. (22) and (23) will be obtained. We, however, did not repeat more than twice since our purpose was not to reporduce the flow curves exactly. The parametric values are tabulated in *Tables* I and II.

**Application of the Flow Equations** Eqs. (22) and (23) were applied to the upcurve and the downcurve, respectively, of the 10.5 wt % of bentonite suspension. The values for $I$, $I'$,

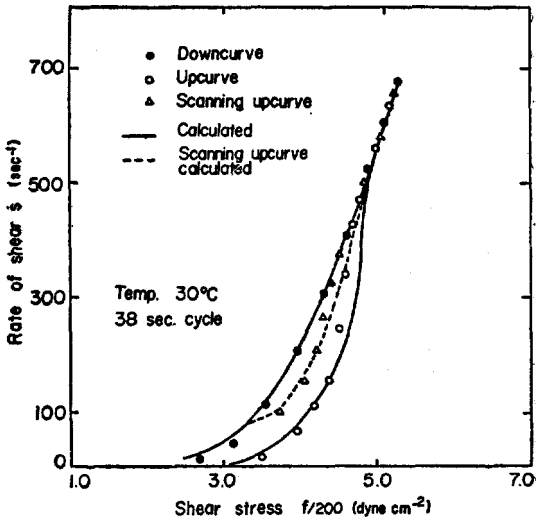


*Fig.* 6. Comparison of observed and calculated flow curves for 10.5 wt. % bentonite suspension.

*Table* I Parametric values of the thixotropic curve for 10.5 wt. % bentonite suspension

| $C'\beta_1/\alpha_1$ dyne cm$^{-2}$ sec. | $\beta_3$ sec. | $\beta_2$ sec. | $X_3/\alpha_3$ dyne cm$^{-2}$ | $C'/\alpha_2$ dyne cm$^{-2}$ | $\gamma$ sec. | $k_f$ sec.$^{-1}$ | $k_b$ sec.$^{-1}$ |
|---|---|---|---|---|---|---|---|
| 0.23 | 2.0 | 0.2 | 112.5 | 92.5 | 10.5 | 0.120 | 0.097 |

*Table* II Parametric values of the thixotropic curve for 9.0 wt. % bentonite suspension containing KCl

| KCl added meq/100ml | $C'\beta_1/\alpha_1$ dyne cm$^{-2}$ sec. | $X_3/\alpha_3$ dyne cm$^{-2}$ | $\beta_3$ sec. | $\beta_2$ sec. | $C'/\alpha_2$ dyne cm$^{-2}$ | $\gamma$ sec. | $k_f$ sec.$^{-1}$ | $k_b$ sec.$^{-1}$ |
|---|---|---|---|---|---|---|---|---|
| 0.0 | 0.02 | 58.0 | 0.075 | 0.01 | 43.0 | 17 | 0.107 | 0.0865 |
| 0.2 | 0.19 | 74.0 | 1.50 | 0.12 | 65.0 | 11.9 | 0.084 | 0.067 |

$J$, $J'$ as well as for the integrals,

$$\int_0^{y} \exp(-y^2)\exp(k_f rI + k_b rI')dy$$

and

$$\int_0^{y'} \exp(-y'^2)\exp(k_f rJ + k_b rJ')dy'$$

were found from the *Tables* prepared.[21] In *Fig.* 6, the results calculated by using the parametric values of *Table* I are compared with experiment; the calculated curves are shown by full and dash curves, the latter being the scanning upcurve. One sees reasonable agreement between theory and experiment.

Equations (22) and (23) were also applied to the flow curves obtained for the electrolyte-treated bentonite suspensions. In *Fig.* 7 are shown two cases: one is the electrolyte-free system of 9.0 wt % bentonite suspension, and the other is the bentonite suspension including KCl (2.0 meq/100 ml). By using the the parametric values for the two systems (*Table* II), the calculated curves were obtained, and are shown by full-curves in *Fig.* 7. Reasonable agreement between theory and experiment is also seen here.

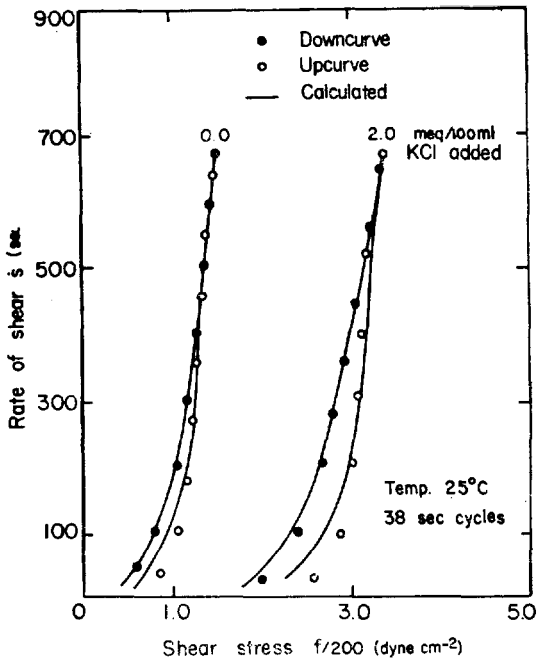


*Fig.* 7. Comparison of observed and calculated flow curves for 9.0 wt. % bentonite suspensions. One system is electrolyte free and the other contains electrolyte (2.0 meq/100 ml KCl).

**The Effects of Electrolyte on the Flow Parameters** When the parametric values (*Table* II) are compared, one finds that all the values, except the last three, *i.e.*, $\gamma$, $k_f$ and $k_b$, are

greater for the electrolyte-treated system than for the original electrolyte free system. The larger values of $X_3/\alpha_3$ and $C'/\alpha_2$ for the electrolyte-treated system may lead to the following facts: (a) The fractional area of type 3 units is increased in the electrolyte-treated suspension due to the flocculation effect of the electrolyte which yields an increased degree of structural formation. Here the intrinsic shear modulus of type 3 unit ($1/\alpha_3$) may be considered as constant independent of electrolyte. (b) An effect similar to (a) may be considered to explain the increase in $C'/\alpha_2$ for the electrolyte-treated system where $C'=X_1+X_2$. Here it is also considered that $1/\alpha_2$ is about independent of electrolyte.

The larger values of $\beta_3$ and $\beta_2$ for the electrolyte-added system indicate that type 3 unit as well as type 2 unit flow more readily in the original electrolyte free suspension than in the electrolyte treated suspension. The increase in $\beta_3$ and $\beta_2$ in the electolyte-treated system is natural, since the attractive forces (van der Waals type) acting on these units increase because of the effect of electrolyte. The decrease of $k_f$ and $k_b$ for the electrolyte-added system is similarly explained.

Next, the values of $\gamma$ will be compared; the value is smaller for the electrolyte-added system than for the original electrolyte free system. We obtain

$$\gamma=\left(\frac{kT}{G}\right)^{\frac{1}{2}}\frac{2k_f}{\rho} \qquad (32)$$

by introducing Eq. (11) into Eq. (17d). If $G$ is considered as constant irrespective of the electrolyte, the decrease in $\gamma$ will be explained by the decrease in $k_f$ for the electrolyte added system [see Eq. (32)]. In fact the ratio $\gamma_o/\gamma_a=17/11.9$ is approximately equal to the ratio $k_{f(o)}/k_{f(a)}=0.107/0.084$ (see *Table* II) where the subscripts $o$ and $a$ indicate the electrolyte-free and the electrolyte-added systems. Here we have assumed that $G$ (shear modulus) is constant independent of electrolyte; based on this fact, we previously assumed that the intrinsic shear moduli $1/\alpha_3$ and $1/\alpha_2$ are assumed to be constant irrespective of the presence of electrolyte.

## Acknowledgment

The authors thank Professor Henry Eyring for invaluable discussions and suggestions. The authors are indebted to Dr. H. Utsugi for his contribution in the conception of this work. The financial assistance for this work was given by the National Science Foundation of the United States Government.

## References

(1) D. M. C. MacEwan, *The X-ray Identification and Crystal Structures of Clay Minerals*, 143-207, ed. by G. Brown, Mineralogical Society, London, 1961, p. 544.

(2) R. E. Grim, *Applied Clay Mineralogy*, pp. 16-20, McGraw-Hill, New York, 1962, p. 422.

(3) T. F. Bates, *Publication of the Mineral Industry Experiment Station*, Pennsylvania State University, Circular No. 51, 1958.

(4) E. A. Hauser and C. E. Reed, *J. Phys. Chem.*, **40**, 1169 (1936).

(5) P. A. Rebinder, *Discussions Faraday Soc.*, **18**, 151 (1954).

(6) C. D. Ripple and P. R. Day, *Clays and Clay Minerals*, Nat. Acad. Sci.-Nat. Res. Council, 14th Conf., 307-316 (1966).

(7) S. Onogi, T. Masuda and T. Matsumoto, *Nippon Kagaku Zasshi*, **88**, 584 (1967).

(8) V. A. Fedotova, Kh. Khodzhaena, and P. A. Rebinder, *Kolloid Zh.*, **30**, 435 (1968).

(9) G. K. Shishkovskii, N. N. Serb-Serbina, N.

B. Urév and P. A. Rebinder, *Dokl. Akad. Nauk.*, **89**, 369 (1969).
(10) G. U. Stratulat, I. N. Vladavets, N. N. Serb-Serbina, and P. A. Rebinder, *Kolloid Zh.*, **32**, 765 (1970).
(11) (a) S. J. Hahn, T. Ree, and H. Eyring, *NLGI Spokesman*, (J. National Lubricating Grease Institute), **21**, 12 (1957); **23**, 129 (1959); *Ind. Eng. Chem.*, **51**, 856 (1959); (b) H. Utsugi, H. Iwasawa, and T. Ree, *Nippon Kagaku Zasshi*, **91**, 690 (1970).
(12) H. Green, *Ind. Eng. Chem., Anal. Ed.*, **14**, 575 (1942).
(13) (a) R. N. Weltmann, *NLGL Spokesman* (J. National Lubricating Grease Institute), **20**, No. 3, 34 (1956); (b) H. Utsugi, K. Kim, T. Ree and H. Eyring, *ibid*, **25**, 125 (1961).
(14) T. Ree and H. Eyring, *Rheology*, ed. by F. R. Eirich, Vol. II, p. 83, Academic Press, New York, 1958, p. 591; J. App. Phys., **26**, 793, 800 (1955).
(15) M. B. M'Ewen and M. I. Pratt, *Trans. Faraday Soc.*, **53**, 535 (1957).
(16) K. Norrish, *Discussions Faraday Soc.*, **18**, 120 (1954).
(17) H. van Olphen, *An Introduction to Clay Colloid Chemistry*, Interscience, New York, 1963, p. 301.
(18) J. L. McAtee, Jr., *Clays and Clay Minerals*, Nat. Res. Council, 5th Conf., 279-288, 1958.
(19) N. Mungan and F. W. Jessen, *Clays and Clay Minerals*, Nat. Acad. Sci. - Nat. Res. Council, 11th Conf., 283-294 (1962).
(20) S. Glasstone, K. J. Laidler and H. Eyring, *The Theory of Rate Processes*, McGraw-Hill, New York, 1941, p. 611.
(21) K. Park, *Thesis*, Department of Metallurgy, University of Utah, Salt Lake City, Utah, U. S. A., 1966.

DAEHAN HWAHAK HWOEJEE
(Journal of the Korean Chemical Society)
Vol. 15, No. 6, 1971
Printed in Republic of Korea

# Effect of Electrolytes on Flow Properties of Aqueous Bentonite Suspension

**Kisoon Park,* Taikyue Ree** and **Henry Eyring**

*Department of Chemistry, University of Utah*
*Salt Lake City, Utah, U. S. A.*

(Received Oct. 21, 1971)

**Abstract** Dependence of the flow behavior of aqueous suspension of Black Hills bentonite on the concentration and the type of electrolytes was studied. The flow properties were measured with a Couette-type rotational viscometer. On addition of monovalent cations, the apparent viscosity determined from the reproducible flow curves (shear rate *vs.* shear stress) decreased followed by a rise as the ionic concentration further increased. Addition of multivalent cations (di- and tri-) resulted in the viscosity which increased to a maximum then decreased to a constant value. Anions of different charges produced essentially the same relationship between viscosity and electrolyte concentration. The flow behavior of the electrolyte-containing suspensions was rationalized in terms of the Derjaguin-Landau-Verwey-Overbeek theory of colloidal stability and the generalized theory of viscosity.

* Present Address: Union Carbide Corporation, Chemicals and Plastics Division, South Charleston, W. Va., U. S. A.